

Hierarchical auxetic and isotropic porous medium with extremely negative Poisson's ratio

Maryam Morvaridi^a, Giorgio Carta^b, Federico Bosia^a, Antonio S. Gliozzi^a,
Nicola M. Pugno^{c,d}, Diego Misseroni^{c,*}, Michele Brun^{b,*}

^a Department of Applied Science and Technology, Politecnico di Torino, Corso Duca degli Abruzzi 24, 10129 Torino, Italy

^b Dipartimento di Ingegneria Meccanica, Chimica e dei Materiali, Università di Cagliari, Piazza d'Armi, 09123 Cagliari, Italy

^c Laboratory of Bio-inspired, Bionic, Nano, Meta Materials & Mechanics, Department of Civil, Environmental and Mechanical Engineering, University of Trento, Via Mesiano 77, 38123 Trento, Italy

^d School of Engineering and Materials Science, Queen Mary University of London, Mile End Road, London E1 4NS, UK



ARTICLE INFO

Article history:

Received 12 April 2021

Received in revised form 22 May 2021

Accepted 24 June 2021

Available online 27 June 2021

Keywords:

Auxetic metamaterial
Negative Poisson's ratio
Hierarchical structure
Porous medium
Experimental validation

ABSTRACT

We propose a novel two-dimensional hierarchical auxetic structure consisting of a porous medium in which a homogeneous matrix includes a rank-two set of cuts characterised by different scales. The six-fold symmetry of the perforations makes the medium isotropic in the plane. Remarkably, the mesoscale interaction between the first- and second-level cuts enables the attainment of a value of the Poisson's ratio close to the minimum reachable limit of -1. The effective properties of the hierarchical auxetic structure are determined numerically, considering both a unit cell with periodic boundary conditions and a finite structure containing a large number of repeating cells. Further, results of the numerical study are validated experimentally on a polymeric specimen with appropriately arranged rank-two cuts, tested under uniaxial tension. We envisage that the proposed hierarchical design can be useful in numerous engineering applications exploiting an extreme auxetic effect.

© 2021 Elsevier Ltd. All rights reserved.

1. Introduction

Auxetic materials are characterised by the unconventional property of possessing an effective negative Poisson's ratio, so that they expand (contract) transversally when stretched (compressed) longitudinally.

Named "auxetic" after Evans [1], these media owe their special behaviour mainly to their microstructure rather than to their chemical composition. Hence, auxeticity has been observed at different scales, from macro- to nano-dimensions. Apart from examples of natural materials with an intrinsic negative Poisson's coefficient [2–5], auxetic media are generally artificially-made systems, whose microstructure is designed by exploiting different geometries and mechanisms: re-entrant unit cells [6–9], star-shaped inclusions [10,11], chiral configurations [12–15], double arrowhead honeycombs [16], perforations and cuttings [17–21], rotating rigid units [22], lattices [23–25] and elastic instabilities [26,27]. Alternative approaches to design auxetic media are presented in the reviews [28–32]. Some auxetic systems are also characterised by a negative value of the coefficient of thermal expansion, implying that they shrink when subjected to an increase

in temperature [33–35]. Additionally, it has been shown that it is also possible to achieve a smooth transition through a wide range of negative and positive Poisson's ratios by using an origami cell that morphs continuously between a Miura mode and an eggbox mode [36–38].

The increasing interest of the scientific community in auxetic metamaterials is due to their enhanced mechanical properties with respect to those of conventional materials, including higher indentation resistance [39] and impact energy absorption abilities [40,41], improved fatigue performance [42] and pull-out strength [43], as well as the possibility to bend with synclastic curvature [44]. For these reasons, auxetic metamaterials have tremendous potential in many fields, particularly in the aviation industry, e.g. for aircraft design [43,45,46], in sports applications for enhanced comfort and protection [47], in electronics to increase electric power output [48] and in biomedical engineering for the design of novel types of stents [49–51] and orthopedic implants [52]. On the other hand, zero Poisson's ratio materials have been shown to be useful in other applications, for instance, in the design of morphing aircraft [53–55].

Hierarchical structures are widely exploited in natural [56] and in bioinspired artificial [57] materials to enhance mechanical properties. The simultaneous presence of multiple length scales, together with material heterogeneity, has been shown to allow the simultaneous optimisation of strength and toughness [58,59],

* Corresponding authors.

E-mail addresses: diego.misseroni@unitn.it (D. Misseroni), mbrun@unica.it (M. Brun).

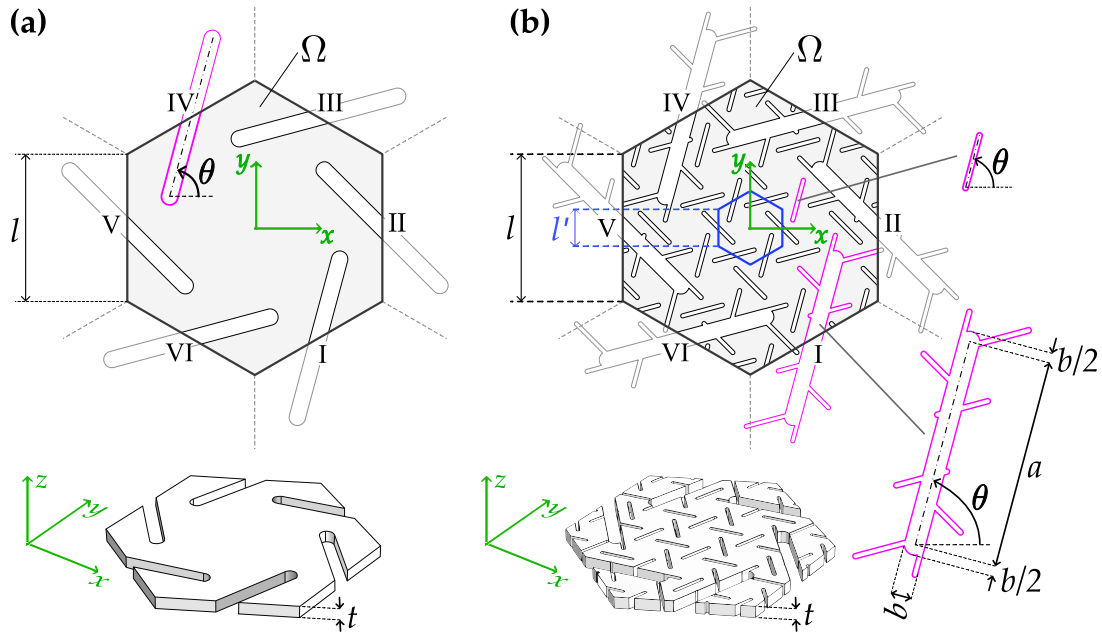


Fig. 1. Top and isometric views of the considered unit cells: (a) non-hierarchical rank-one hexagonal unit cell; (b) hierarchical rank-two unit cell, with additional second-level cuts.

but also to enable the improvement of other mechanical characteristics such as adhesion [60,61], friction [62], or to achieve band gap engineering in dynamics [63,64].

In this paper, we investigate the auxetic behaviour of a porous hierarchical medium, consisting of a homogeneous elastic material containing two classes of perforations, characterised by two different length scales and exhibiting a six-fold symmetry, which makes the medium isotropic [65,66]. First, by numerically studying the periodic elementary cell, we demonstrate that, for some ratios between the lengths of the two classes of cuts, the effective Poisson's ratio approaches the limit of -1 . Second, we verify the results of the periodic analysis by determining the response of a finite model, containing a large number of periodic cells, under uniaxial loading. Subsequently, we validate the numerical results by experimentally testing a specimen with hierarchical cuts in uniaxial tension. Finally, we provide some analysis and concluding remarks.

2. Numerical model

We introduce a 2-D hexagonal periodic unit cell with oriented cuts, as shown in Fig. 1a. The cuts are all rotated by the same relative angle θ ($\theta = \pi/6$ with respect to the intersected edge of the hexagonal unit cell of size l). Each cut is of length a and width b , which is also the diameter of the rounded extremities (in consideration of a practical realisation). The proposed design leads to a periodic pattern with either six-fold or three-fold symmetry, similar to previously considered designs providing an isotropic auxetic response [19,20].

Next, we construct a second-rank geometry by adding smaller cuts to the first, arranged periodically in a hexagonal pattern of size l' and in turn oriented at the same angle θ (Fig. 1b). This entails the introduction of a second characteristic size scale in the system, leading to a so-called ‘‘hierarchical’’ geometry. The transposition of these 2-D geometries in real 3-D structures is implemented in thin sheets of thickness t , shown in the bottom panels of Fig. 1.

We numerically evaluate the quasi-static behaviour under uniaxial tension of the two proposed 2-D geometries. For both,

we derive the ‘‘effective’’ properties as functions of the geometric parameters. This is accomplished by performing a Finite Element (FE) analysis using the commercial package *COMSOL Multiphysics*[®] (version 5.6). A state of plane stress is assumed in the numerical simulations and periodic boundary conditions are applied at the edges of the unit cell. Geometrical parameters are taken as follows: cut length $a = 10$ mm, cut width $b = 1$ mm, lengths of the hexagonal cells $l = 9.00$ mm and $l' = 2.25$ mm, Young's modulus $E = 2.285$ GPa and Poisson's coefficient $\nu = 0.37$.

The effective elastic properties of the structure are derived by applying macroscopic longitudinal strains in the horizontal ($\varepsilon_{xx} = 10^{-4}$) and vertical ($\varepsilon_{yy} = 10^{-4}$) directions and the macroscopic shear strain $\varepsilon_{xy} = 10^{-4}$. Each of these macroscopic strains is applied to the unit cell using periodic boundary conditions. Specifically, periodic boundary conditions link displacements on edges having opposite outward normal unit vectors. Referring to Fig. 1, the periodic boundary conditions satisfy the relations $u_i^{(\alpha)} - u_i^{(\alpha+III)} = \varepsilon_{ij} (X_j^{(\alpha)} - X_j^{(\alpha+III)})$, where $\alpha = I, II, III$ while u_i are the displacements, X_j the positions and $i, j = x, y$. In the numerical computations, additional constraints are imposed to prevent rigid-body motions. The macroscopic Cauchy stress components σ_{xx} , σ_{yy} and σ_{xy} are evaluated numerically as average values of the corresponding local components s_{xx} , s_{yy} and s_{xy} on the unit cell domains of the models, namely:

$$\sigma_{ij} = \frac{1}{|\Omega|} \int_{\Omega} s_{ij} \, d\mathbf{x} = (1-p) \sigma_{ij}^{(S)} + p \sigma_{ij}^{(P)} = (1-p) \sigma_{ij}^{(S)} \quad (ij = xx, yy, xy), \quad (1)$$

where Ω is the unit cell domain, $\sigma_{ij}^{(S)}$ and $\sigma_{ij}^{(P)} = 0$ are the average stresses in the solid (S) and porous (P) phases, respectively, and p is the porosity.

From these values, it is possible to estimate the effective Young's modulus E_{eff} and Poisson's ratio ν_{eff} for plane stress conditions. From Hooke's law, the effective properties of an isotropic material are given by (see Appendix A)

$$E_{eff} = \frac{\sigma_{xx}^2 - \sigma_{yy}^2}{\varepsilon_{xx} \sigma_{xx} - \varepsilon_{yy} \sigma_{yy}}, \quad (2)$$

$$\nu_{eff} = \frac{\varepsilon_{xx}\sigma_{yy} - \varepsilon_{yy}\sigma_{xx}}{\varepsilon_{xx}\sigma_{xx} - \varepsilon_{yy}\sigma_{yy}}, \quad (3)$$

$$\mu_{eff} = \frac{\sigma_{xy}}{2\varepsilon_{xy}} = \frac{E_{eff}}{2(1 + \nu_{eff})}. \quad (4)$$

The equations above provide the homogenised properties of the 2-D linear elastic material, characterised by six-fold or three-fold symmetry. The FE simulations, performed with the three imposed strain components indicated above, confirm the isotropic behaviour of the structure, for both the hierarchical and non-hierarchical designs (the detailed analysis is reported in Appendix A). The local von Mises stress distributions s_{VM} for both the non-hierarchical and hierarchical models, under the three strain conditions, are illustrated in Fig. 2. The local stress field components s_{xx} , s_{yy} and s_{xy} are also shown in Appendix B.

The effective Young's modulus and Poisson's ratio obtained for the non-hierarchical geometry are $E_{eff} = 201$ MPa and $\nu_{eff} = -0.55$ (NHEP: Non-Hierarchical Effective Properties), confirming the auxetic behaviour of this design. In the case of the hierarchical geometry, taking $l = 4l'$, we obtain $E_{eff} = 2.92$ MPa and $\nu_{eff} = -0.92$, i.e. there is a considerable reduction in the stiffness, but also a remarkable increase in the auxetic behaviour, with an effective Poisson's ratio tending to the minimum reachable value -1. Thus, as assumed, the hierarchical structure can yield a considerable variation in the mechanical properties of architected structures, with the possibility of achieving extreme values. Notice that, despite a reduction in effective Young's modulus between the hierarchical and non-hierarchical case, stress levels remain comparable, due to high stress concentrations at the tips of the cuts; the maximum local von Mises stresses are reported in Tables A.1 and A.2 in Appendix A.

These properties are strongly dependent on the choice of the microstructural geometrical parameters, in particular the so-called "hierarchical ratio" between the characteristic size of each rank of cuts. Therefore, we evaluate the variation of the mechanical properties of the structure (E_{eff} and ν_{eff}) with respect to the hierarchical ratio $s = l'/l$, for values ranging between 1/18 and 1/2. For each hierarchical geometry, the centre of the unit cell of the rank-one system of cuts coincides with the centre of the central unit cell of the rank-two system of cuts in order to enforce the overall six-fold symmetry.

Results are detailed in Table 1 and shown graphically in Fig. 3, together with the effective properties of the non-hierarchical structure (NHEP – horizontal blue lines) and of the "Matrix with effective properties" (MEP – horizontal red lines). In the computations, the hierarchical structure corresponding to MEP has been implemented as a non-hierarchical geometry, and the local properties of the matrix phase have been taken as the effective properties of the non-hierarchical system (NHEP). When the hierarchical ratio $s \rightarrow 0^+$, separation of length scales holds between the local perturbations of the fields (stress and strain) induced by the two ranks of cuts. In such a case, it is justified to model the matrix phase as a homogeneous material with effective properties instead of introducing rank-two cuts.

Fig. 3 confirms that decreasing the hierarchical ratio s , both the Young's modulus and the Poisson's ratio converge to the limiting values corresponding to MEP ($E_{eff} = 17.64$ MPa and $\nu_{eff} = -0.632$). On the other hand, for larger ratios $s \in [1/6, 1/2]$ the numerical results show large oscillations of the elastic properties. Remarkably, the Poisson's ratio is minimised at the mesoscale, where the two scales associated with the two ranks of cuts strongly interact locally. Combining the effect of hierarchy and scale interaction constructively, the minimum values of Poisson's ratio are found for $s = 1/6$ and $s = 1/4$, reaching in the latter case

Table 1

Numerically calculated effective Young's modulus, Poisson's ratio and porosity for varying hierarchical ratio $s = l'/l$. In (*) a supercell made of 2×2 cells was analysed to include an integer number of rank-two cells of size l' .

s	E_{eff} (MPa)	ν_{eff}	Porosity (%)
1/2	6.33	-0.03	27
1/3	36.5	-0.22	24
1/4	2.92	-0.92	28
1/5	11.3	-0.60	25
1/5.5 (*)	16.9	-0.50	29
1/6	4.22	-0.85	23
1/6.5 (*)	16.1	-0.58	28
1/7	12.1	-0.62	24
1/8	19.4	-0.61	29
1/9	18.8	-0.55	26
1/12	17.2	-0.58	28
1/15	14.2	-0.63	28
1/18	15.7	-0.62	27
0^+	17.6	-0.63	29

Table 2

Effective Young's modulus and Poisson's ratio for multiple-rank microstructures and $s \rightarrow 0^+$.

Rank	E_{eff} (MPa)	ν_{eff}
1	2285	0.370
2	201	-0.551
3	17.6	-0.632
4	1.55	-0.639
5	0.136	-0.640
6	0.012	-0.640

the value $\nu_{eff} = -0.92$, which is very close to the thermodynamic limit for constitutive stability $\nu_{eff} = -1$. Clearly, the introduction of the second rank of cuts increases the effective porosity and, as expected, causes a decrease in the Young's modulus with respect to the non-hierarchical model. Notice that the exceptional value of ν_{eff} does not depend on the particularly small value of $E_{eff} = 2.92$ MPa for this geometry: calculations for a non-hierarchical unit cell with $E = E_{eff}$ yield $\nu_{eff} = -0.55$.

Concerning the potential benefits of a multiple-rank microstructure, we note that the results for the hierarchical ratio $s = 1/4$ are already close to the limiting value -1. Additional computations under the separation of length scale hypothesis, i.e. iterating the MEP scheme, are reported in Table 2. They show that additional hierarchical levels lead to a small decrease in Poisson's ratio at the cost of a strong reduction of Young's modulus, which is accompanied by additional technological difficulties in specimen manufacture.

To further verify the auxetic behaviour of the proposed design, we study a finite two-dimensional model of dimensions 280×600 mm, including numerous unit cells, under plane stress conditions. With this model, we check that the effective values of Young's modulus and Poisson's ratio at this scale coincide with those estimated for a single periodic unit cell. Again, we consider the structure corresponding to a hierarchical ratio $s = 1/4$ and we apply uniaxial tension to the specimen in the vertical direction, free boundary conditions on the lateral sides, and we evaluate the corresponding horizontal and vertical displacement fields (Fig. 4). The effective Young's modulus and Poisson's ratio are evaluated using Eqs. (2) and (3), where the effective strain and stress components are computed averaging the corresponding local fields in the domain enclosed in the rectangle R indicated by a black line in Fig. 4. Additionally, the effective Poisson's ratio is also determined as the (negative) ratio between the average strains in the horizontal (ε_{xx}) and vertical (ε_{yy}) directions, evaluated from the average horizontal displacements computed on the vertical lines connecting points 1–6 and 3–8 and from the average vertical displacements calculated on the horizontal lines connecting

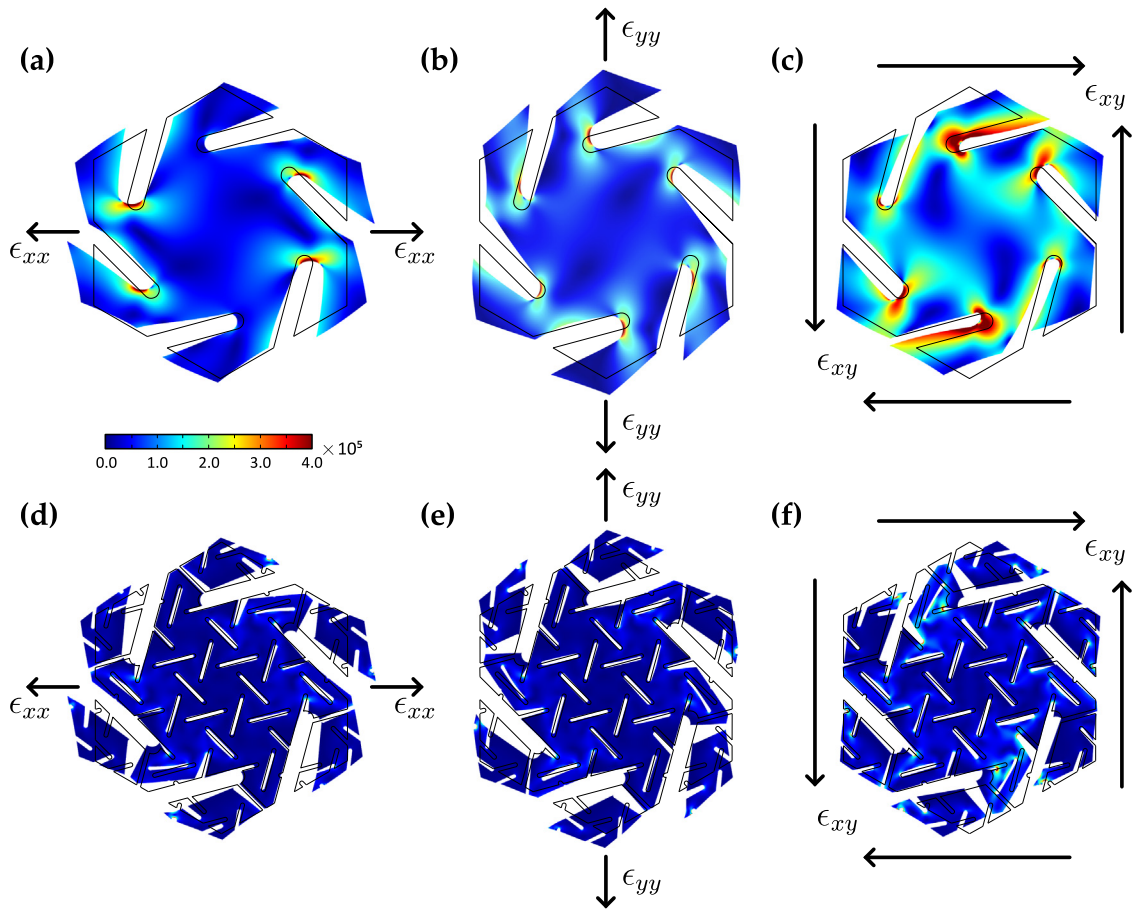


Fig. 2. FE simulations on (a–c) non-hierarchical and (d–f) hierarchical unit cells. (a), (d): normal strain applied in the horizontal direction $\epsilon_{xx} = 10^{-4}$; (b), (e): normal strain applied in the vertical direction $\epsilon_{yy} = 10^{-4}$; (c), (f): shear strain $\epsilon_{xy} = 10^{-4}$. Resulting von Mises stress distributions are represented in colour scale, where the values are given in N/m^2 . For comparison purposes the fields have been plotted with the same colour scale.

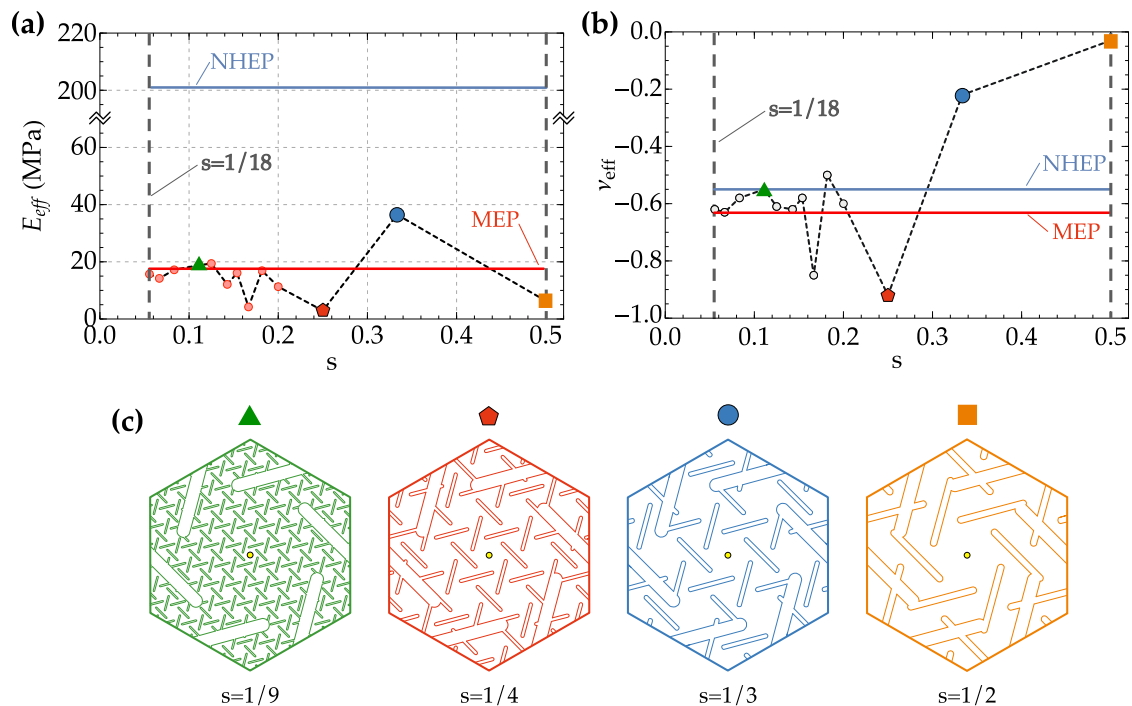


Fig. 3. (a) Effective Young's modulus (note the jump in the scale on the vertical axis) and (b) effective Poisson's ratio of hierarchical-auxetic material as function of hierarchical ratio s . Four of the considered hierarchical auxetic structures are also shown in panel (c).

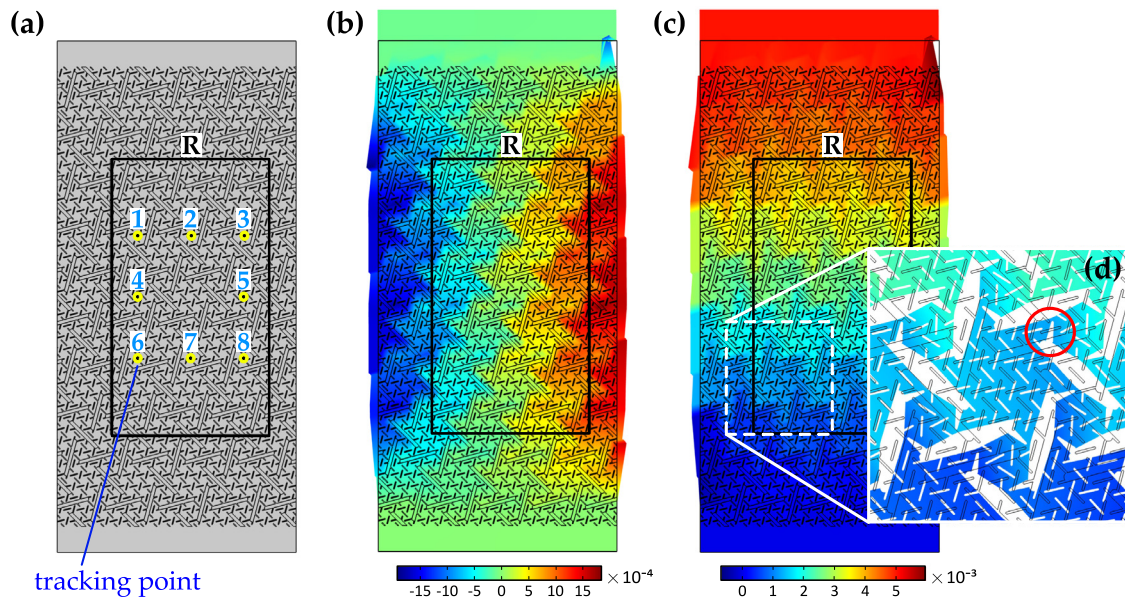


Fig. 4. (a) Considered large-scale geometry. The rectangle R indicates the region where average values of stress and strain are computed for the evaluation of the effective properties. (b) Horizontal and (c) vertical displacements (given in metres) for an applied vertical displacement at the top side of the sample. The displacement components are given in colour scales on the deformed sample. (d) Close-up of unit cell deformation.

points 1–3 and 6–8, respectively (specified in Fig. 4a). The latter approach is implemented to mimic the experimental procedure detailed below (see Fig. 5c). The two approaches yield values of Poisson's ratio which are the same up to the second decimal digit. The resulting effective Young's modulus and Poisson's ratio values are $E_{eff} = 2.9$ MPa and $\nu_{eff} = -0.90$, showing an excellent agreement with previously calculated values for single periodic unit cells.

The contour plots in Fig. 4b and c clearly show the material expansion in the horizontal and vertical directions, demonstrating a large negative Poisson's ratio value. In the close-up in Fig. 4d it is possible to note the scale interaction effect in the strongly deformed rank-two cuts intersecting the larger ones. The red circle in Fig. 4d highlights the large deformation of a rank-two cut, which constructively interacts with the deformations of the adjacent bigger cuts, enhancing the macroscopic auxetic effect.

3. Experimental testing and validation

Experiments were performed to validate the extreme auxetic behaviour of the described hierarchical plate. A thin $280.2 \times 599.8 \times 2$ mm³ PolyCarbonate (PC) specimen with the designed hierarchical distribution of traversing cuts was produced by a Roland EGX-600 engraving machine (accuracy 0.01 mm). The chosen geometry corresponds to a hierarchical ratio $s = 1/4$. The length of the rank-two cuts was reduced by 13% with respect to the geometry considered in Figs. 3 and 4, to avoid exceedingly thin connecting regions between cuts and high stress concentrations, and to make the experiments practically realisable. To mimic the real experiment, an additional numerical simulation of a two-dimensional model under plane stress conditions is performed in *Comsol Multiphysics* considering the same geometry of the specimen tested experimentally.

The specimen is mounted vertically in a loading frame (Messphysick MIDI 10) by uniformly clamping its upper and lower edges, and uniaxial tension is applied, as shown in Fig. 5. During the test, the load is acquired with a DCSRC - 1 kN load cell and the displacement with a displacement transducer mounted in the loading frame. Small dots (0.5 mm in diameter) drawn at specific locations on the sample are used as tracking markers (also shown

in Fig. 5c), and a 4K Sony PXW-F55 (3840×2160 pixel) camera is used to track their displacements during loading (see the movie in the Supplementary Material).

Results are shown in Fig. 5a: a vertical displacement is applied to the top of the specimen up to $u_{y,max} = 6$ mm, and a perfectly linear elastic response is detected, leading to the estimation of an effective Young's modulus of 3.33 MPa. In the figure, the loading/unloading curve shows the perfectly linear elastic response of the specimen. To estimate the experimental average value of the Poisson's ratio, 8 markers are placed along the edges of a rectangular region in the central area of the hierarchical plate, as shown in Fig. 5c. The average horizontal and vertical displacements measured by using the 8 tracking points allow to estimate the Poisson's ratio that, after an initial variation due to specimen adjustment, tends to a value of $\bar{\nu} \cong -0.84$ (Fig. 5b). Such a value is in excellent agreement with the numerical value $\nu_{eff} = -0.86$, obtained with a finite numerical model analysed in *Comsol Multiphysics* and having the same geometry as the specimen tested in the lab.

4. Conclusions

In conclusion, we have designed and tested a simple 2-D structure consisting of a hierarchical arrangement of rotated thin cuts, which displays extreme auxetic properties along each of its 6-fold symmetry directions, providing an isotropic architecture. The novelty of this structure is that it effectively expands uniformly in the plane when loaded uniaxially in any direction.

The design procedure starts from a previously considered single scale (non-hierarchical) design, adding smaller symmetrically rotated cuts, thus introducing an additional scale level into the structure. First, we show that this structure can be treated macroscopically as an isotropic homogeneous medium, with calculated effective quasi-static mechanical properties. Simulations show that these properties are susceptible to geometrical parameters, in particular the ratio between the lengths of the first- and second-rank unit cells. The designed structure enables a kirigami-like behaviour, and, by exploiting the interaction between the

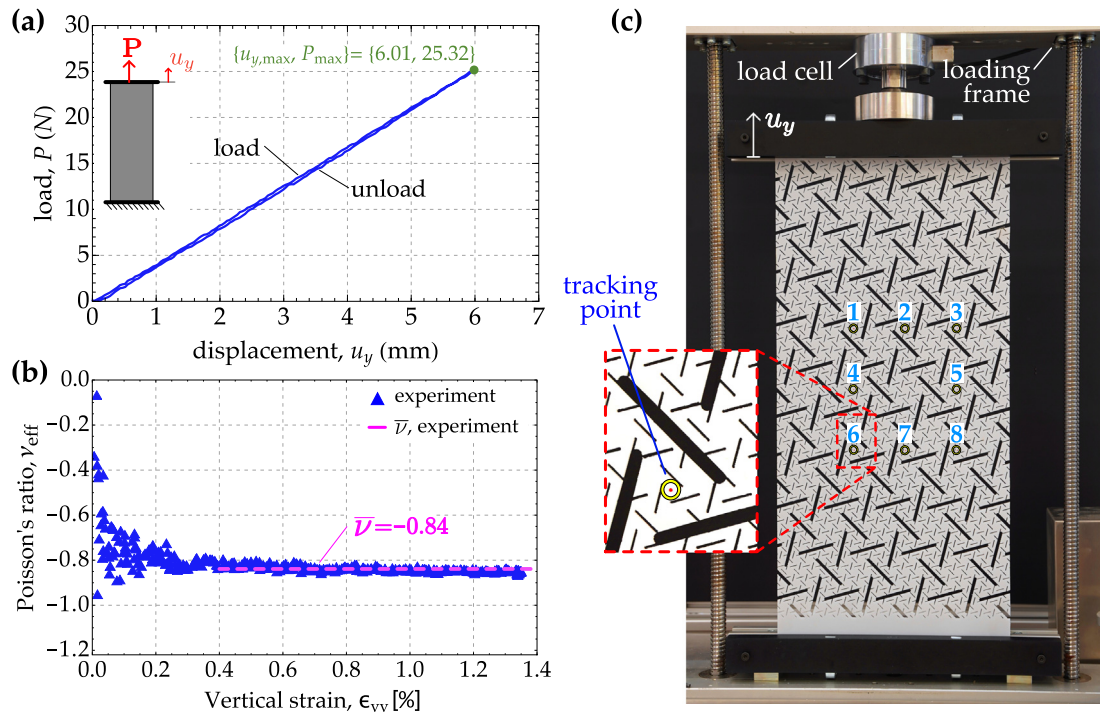


Fig. 5. (a) Force vs. displacement diagram (loading/unloading curve) recorded during the experimental test. (b) Effective Poisson's ratio as a function of the vertical strain. The blue/triangle markers and the dashed/magenta line represent the experimental Poisson's ratio and its average value, respectively. (c) Experimental setup, with the specimen inside the loading frame. The tracking markers exploited to estimate the Poisson's ratio are highlighted and labelled from 1 to 8. An example of tracking marker is also highlighted in the inset.

scales, it is possible to achieve extreme isotropic auxetic properties. Numerical predictions are verified by experimental tests with a large degree of confidence.

Future work will focus on a better understanding of the variation of effective mechanical properties of the proposed structures as a function of geometrical parameters, including the introduction of further hierarchical levels.

The designed auxetic structures can be beneficial for many applications in the biomedical field (e.g. for the design of novel types of stents), in the fabrication of impact protection devices and of robust shock and sound-absorbing materials, as well as in the textile industry for the development of new fabrics.

Declaration of competing interest

The authors declare that they have no known competing financial interests or personal relationships that could have appeared to influence the work reported in this paper.

Acknowledgements

MM, FB, ASG, DM and NMP are supported by the European Commission under the H2020 FET Open ("Boheme") grant No. 863179. MB acknowledges the financial support of Regione Autonoma della Sardegna, Italy, project ADVANCING.

Appendix A. Numerical verification of the isotropy of the hierarchical auxetic medium

Hooke's law for a linear elastic isotropic medium under plane stress conditions can be expressed as follows:

$$\varepsilon_{xx} = \frac{\sigma_{xx} - \nu_{eff}\sigma_{yy}}{E_{eff}}, \quad (\text{A.1})$$

Table A.1

Non-hierarchical geometry. Average values of stress and strain components and maximum value of von Mises stress obtained from three separate numerical computations.

Case	Applied strains			Calculated stresses (Pa)			
	ε_{xx}	ε_{yy}	ε_{xy}	σ_{xx}	σ_{yy}	σ_{xy}	$S_{VM,max}$
(1)	10^{-4}	0	0	28 838	-15 894	0	$0.723 \cdot 10^6$
(2)	0	10^{-4}	0	-15 894	28 838	0	$0.621 \cdot 10^6$
(3)	0	0	10^{-4}	0	0	44 732	$0.930 \cdot 10^6$

Table A.2

Hierarchical geometry. Average values of stress and strain components and maximum value of von Mises stress from three separate numerical computations.

Case	Applied strains			Calculated stresses (Pa)			
	ε_{xx}	ε_{yy}	ε_{xy}	σ_{xx}	σ_{yy}	σ_{xy}	$S_{VM,max}$
(1)	10^{-4}	0	0	1860.0	-1707.9	0	$1.589 \cdot 10^6$
(2)	0	10^{-4}	0	-1707.9	1860.0	0	$1.403 \cdot 10^6$
(3)	0	0	10^{-4}	0	0	3567.9	$2.236 \cdot 10^6$

$$\varepsilon_{yy} = \frac{\sigma_{yy} - \nu_{eff}\sigma_{xx}}{E_{eff}}. \quad (\text{A.2})$$

Eqs. (A.1) and (A.2) can be solved in terms of the effective properties E_{eff} and ν_{eff} , yielding the expressions in Eqs. (2) and (3).

The isotropy of the solid phase and the six-fold symmetry of the geometry of the microstructure assure the isotropy of the effective constitutive properties. As an additional numerical check, we have performed three separate computations imposing three different macroscopic strain components, i.e. $\varepsilon_{xx}^{(1)} = 10^{-4}$, $\varepsilon_{yy}^{(2)} = 10^{-4}$ and $\varepsilon_{xy}^{(3)} = 10^{-4}$. The superscripts (1), (2) and (3) are introduced to distinguish the results of the three different computations.

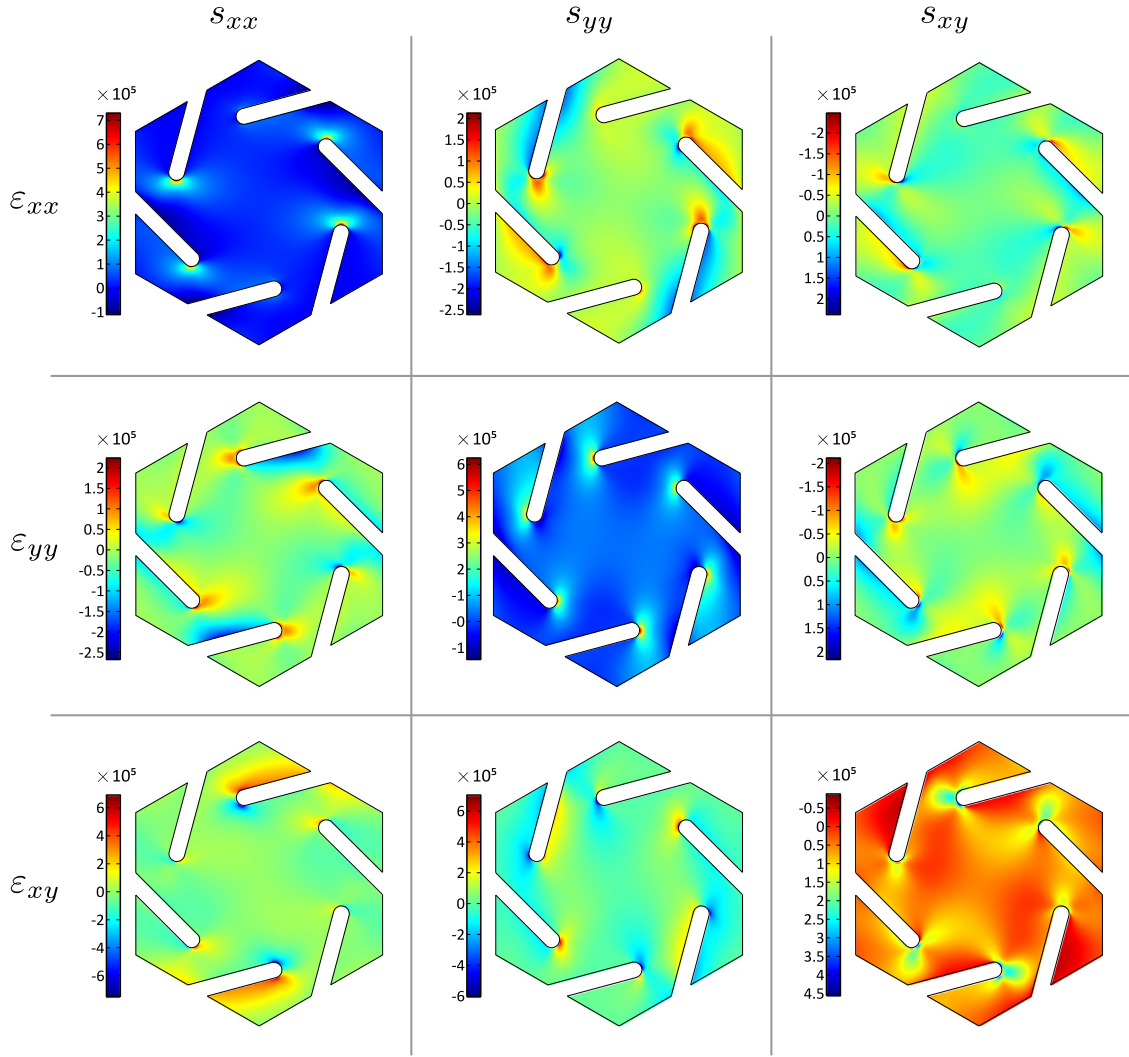


Fig. B.1. Non-hierarchical geometry. Local stress fields in the unit cell for different applied average strains as in Fig. 2 and Tables A.1 and A.2.

We start from a generic orthotropic material under plane stress conditions, for which Hooke's law has the form

$$\varepsilon_{xx} = \frac{\sigma_{xx}}{E_{x,eff}} - \frac{\nu_{yx,eff} \sigma_{yy}}{E_{y,eff}}, \quad (\text{A.3})$$

$$\varepsilon_{yy} = \frac{\sigma_{yy}}{E_{y,eff}} - \frac{\nu_{xy,eff} \sigma_{xx}}{E_{x,eff}}, \quad (\text{A.4})$$

$$\varepsilon_{xy} = \frac{\sigma_{xy}}{2\mu_{xy,eff}}. \quad (\text{A.5})$$

From the first computation, where $\varepsilon_{xx}^{(1)} = 10^{-4}$ and $\varepsilon_{yy}^{(1)} = 0$, we obtain the stress components $\sigma_{xx}^{(1)}$ and $\sigma_{yy}^{(1)}$, which are inserted into Eqs. (A.3) and (A.4). Then, we repeat the same procedure for the second computation, where $\varepsilon_{xx}^{(2)} = 0$ and $\varepsilon_{yy}^{(2)} = 10^{-4}$. Successively, we solve the algebraic system of four equations, which yield

$$E_{x,eff} = \frac{\sigma_{xx}^{(1)} \sigma_{yy}^{(2)} - \sigma_{yy}^{(1)} \sigma_{xx}^{(2)}}{\varepsilon_{xx}^{(1)} \sigma_{yy}^{(2)}}, \quad (\text{A.6})$$

$$E_{y,eff} = \frac{\sigma_{xx}^{(1)} \sigma_{yy}^{(2)} - \sigma_{yy}^{(1)} \sigma_{xx}^{(2)}}{\varepsilon_{yy}^{(2)} \sigma_{xx}^{(1)}}, \quad (\text{A.7})$$

$$\nu_{xy,eff} = \frac{\varepsilon_{yy}^{(2)} \sigma_{yy}^{(1)}}{\varepsilon_{xx}^{(1)} \sigma_{yy}^{(2)}}, \quad (\text{A.8})$$

$$\nu_{yx,eff} = \frac{\varepsilon_{xx}^{(2)} \sigma_{xx}^{(1)}}{\varepsilon_{yy}^{(2)} \sigma_{xx}^{(1)}}. \quad (\text{A.9})$$

The results of the numerical simulations give $\sigma_{xx}^{(1)} = \sigma_{yy}^{(2)}$ and $\sigma_{yy}^{(1)} = \sigma_{xx}^{(2)}$ (see Tables A.1 and A.2), hence we retrieve $E_{x,eff} = E_{y,eff} = E_{eff}$ and $\nu_{xy,eff} = \nu_{yx,eff} = \nu_{eff}$, which can be computed using Eqs. (2) and (3), respectively. This restricts the orthotropic behaviour to a cubic one.

From the third simulation, where $\varepsilon_{xy}^{(3)} = 10^{-4}$, we determine $\sigma_{xy}^{(3)}$ and, using Eq. (A.5), we find $\mu_{xy,eff}$. Since $\mu_{xy,eff} = E_{eff} / (2(1 + \nu_{eff}))$, we verify that the medium is isotropic.

In Tables A.1 and A.2 we report the average values of stresses and strains obtained from the numerical calculations for the non-hierarchical and the hierarchical geometries, respectively.

Appendix B. Stress fields in the hierarchical and non-hierarchical geometry

In Figs. B.1 and B.2, we report the local stress fields components s_{xx} , s_{yy} and s_{xy} in the unit cell for the non-hierarchical

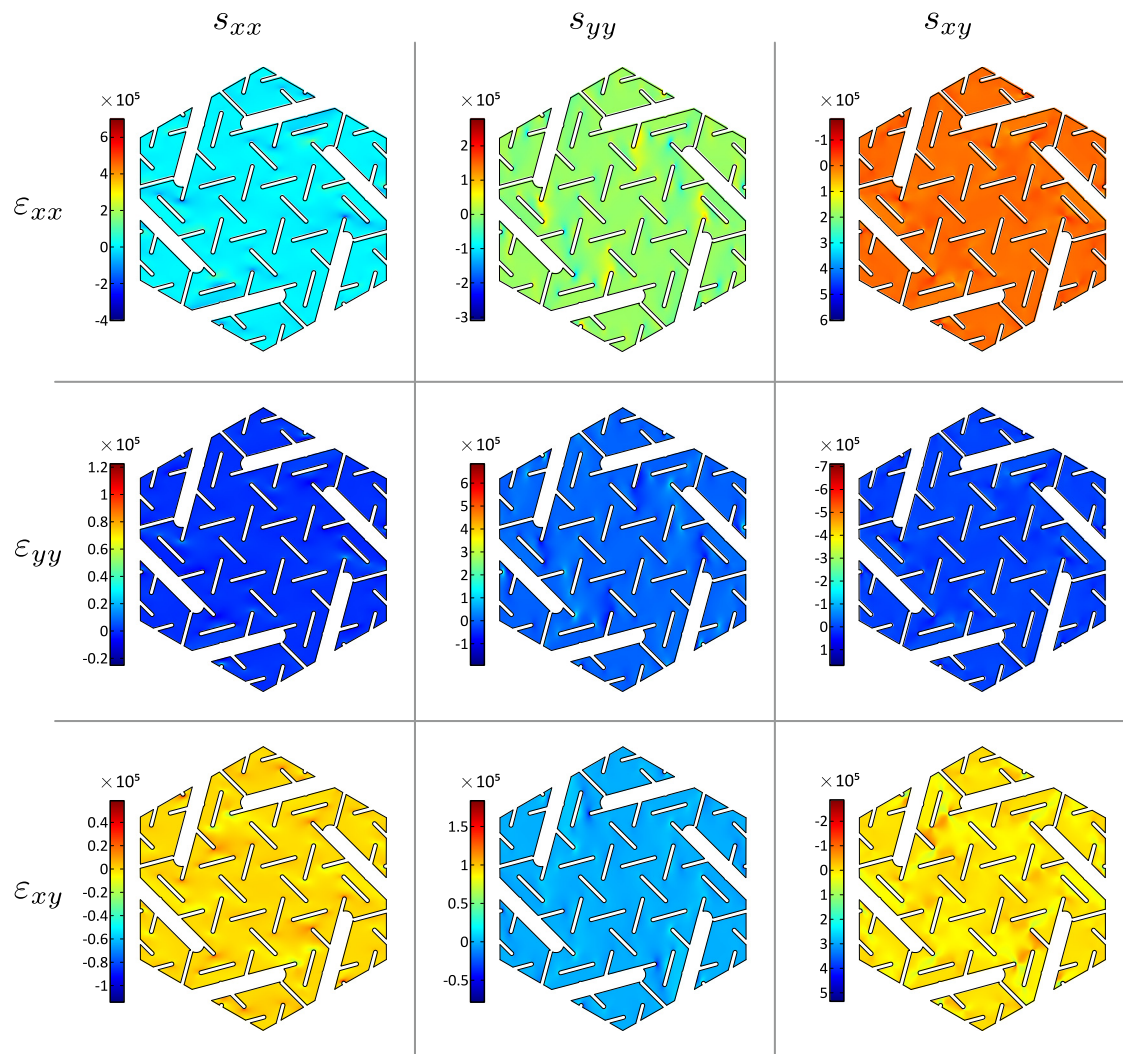


Fig. B.2. Hierarchical geometry. Local stress fields in the unit cell for different applied average strains as in Fig. 2 and Tables A.1 and A.2.

and hierarchical geometries, respectively. Results correspond to applied macroscopic strains as in Fig. 2 and Tables A.1 and A.2.

Appendix C. Supplementary data

Supplementary material related to this article can be found online at <https://doi.org/10.1016/j.eml.2021.101405>.

References

- [1] K.E. Evans, Auxetic polymers: a new range of materials, *Endeavour* 15 (4) (1991) 170–174.
- [2] A. Yeganeh-Haeri, D.J. Weidner, J.B. Parise, Elasticity of α -cristobalite: a silicon dioxide with a negative Poisson's ratio, *Science* 257 (1992) 650–652.
- [3] R.H. Baughman, J.M. Shacklette, A.A. Zakhidov, S. Stafström, Negative Poisson's ratio as a common feature of cubic metals, *Nature* 392 (1998) 362–365.
- [4] J.N. Grima, R. Jackson, A. Alderson, K.E. Evans, Do zeolites have negative Poisson's ratios? *Adv. Mater.* 12 (2000) 1912–1918.
- [5] F. Song, J. Zhou, X. Xu, Y. Xu, Y. Bai, Effect of a negative Poisson ratio in the tension of ceramics, *Phys. Rev. Lett.* 100 (2008) 245502.
- [6] R.S. Lakes, Foam structures with a negative Poisson's ratio, *Science* 235 (1987) 1038–1040.
- [7] C. Lira, P. Innocenti, F. Scarpa, Transverse elastic shear of auxetic multi re-entrant honeycombs, *Compos. Struct.* 90 (3) (2009) 314–322.
- [8] X. Li, Q. Wang, Z. Yang, Z. Lu, Novel auxetic structures with enhanced mechanical properties, *Extreme Mech. Lett.* 27 (2019) 59–65.
- [9] X.-L. Peng, C. Soyarslan, S. Bargmann, Phase contrast mediated switch of auxetic mechanism in composites of infilled re-entrant honeycomb microstructures, *Extreme Mech. Lett.* 35 (2020) 100641.
- [10] P. Theocaris, G. Stavroulakis, P. Panagiotopoulos, Negative Poisson's ratios in composites with star-shaped inclusions: a numerical homogenization approach, *Arch. Appl. Mech.* 67 (1997) 274–286.
- [11] L. Mizzi, E.M. Mahdi, K. Titov, R. Gatt, D. Attard, K.E. Evans, J.N. Grima, J.-C. Tan, Mechanical metamaterials with star-shaped pores exhibiting negative and zero Poisson's ratio, *Mater. Des.* 146 (2018) 28–37.
- [12] D. Prall, R.S. Lakes, Properties of a chiral honeycomb with a Poisson's ratio of -1, *Int. J. Mech. Sci.* 39 (1997) 305–314.
- [13] J.N. Grima, R. Gatt, P.S. Farrugia, On the properties of auxetic meta-tetrachiral structures, *Phys. Status Solidi b* 245 (3) (2008) 511–520.
- [14] A. Spadoni, M. Ruzzene, Elasto-static micropolar behavior of a chiral auxetic lattice, *J. Mech. Phys. Solids* 60 (1) (2012) 156–171.
- [15] A. Bacigalupo, L. Gambarotta, Chiral two-dimensional periodic blocky materials with elastic interfaces: Auxetic and acoustic properties, *Extreme Mech. Lett.* 39 (2020) 100769.
- [16] U.D. Larsen, O. Sigmund, S. Bouwsta, Design and fabrication of compliant micro-mechanisms and structures with negative Poisson's ratio, *J. Microelectromech. Syst.* 6 (1997) 99–106.
- [17] J.N. Grima, R. Gatt, Perforated sheets exhibiting negative Poisson's ratios, *Adv. Eng. Mater.* 12 (6) (2010) 460–464.
- [18] M. Taylor, L. Francesconi, M. Gerends, A. Shanian, C. Carson, K. Bertoldi, Low porosity metallic periodic structures with negative Poisson's ratio, *Adv. Mater.* 26 (15) (2014) 2365–2370.
- [19] S. Shan, S.H. Kang, Z. Zhao, L. Fang, K. Bertoldi, Design of planar isotropic negative Poisson's ratio structures, *Extreme Mech. Lett.* 4 (2015) 96–102.
- [20] G. Carta, M. Brun, A. Baldi, Design of a porous material with isotropic negative Poisson's ratio, *Mech. Mater.* 97 (2016) 67–75.

- [21] F. Box, C.G. Johnson, D. Pihler-Puzović, Hard auxetic metamaterials, *Extreme Mech. Lett.* 40 (2020) 100980.
- [22] J.N. Grima, A. Alderson, K.E. Evans, Auxetic behaviour from rotating rigid units, *Phys. Status Solidi b* 242 (3) (2005) 561–575.
- [23] L. Cabras, M. Brun, Auxetic two-dimensional lattices with Poisson's ratio arbitrarily close to -1 , *Proc. R. Soc. Lond. A* 470 (2172) (2014) 20140538.
- [24] L. Cabras, M. Brun, A class of auxetic three-dimensional lattices, *J. Mech. Phys. Solids* 91 (2016) 56–72.
- [25] X. Chen, J. Moughames, Q. Li, J.A.I. Martínez, H. Tan, S. Adrar, N. Laforge, J.-M. Cote, S. Euphrasie, G. Ulliac, M. Kadic, V. Laude, Optimal isotropic, reusable truss lattice material with near-zero Poisson's ratio, *Extreme Mech. Lett.* 41 (2020) 101048.
- [26] K. Bertoldi, P.M. Reis, S. Willshaw, T. Mullin, Negative Poisson's ratio behavior induced by an elastic instability, *Adv. Mater.* 22 (3) (2010) 361–366.
- [27] J. Shen, S. Zhou, X. Huang, Y.M. Xie, Simple cubic three-dimensional auxetic metamaterials, *Phys. Status Solidi b* 251 (8) (2014) 1515–1522.
- [28] Y. Prawoto, Seeing auxetic materials from the mechanics point of view: A structural review on the negative Poisson's ratio, *Comput. Mater. Sci.* 58 (2012) 140–153.
- [29] K.K. Saxena, R. Das, E.P. Calius, Three decades of auxetics research – materials with negative Poisson's ratio: A review, *Adv. Eng. Mater.* 18 (2016) 11.
- [30] H.M.A. Kolken, A.A. Zadpoor, Auxetic mechanical metamaterials, *RSC Adv.* 7 (2017) 5111–5129.
- [31] X. Ren, R. Das, P. Tran, T.D. Ngo, Y.M. Xie, Auxetic metamaterials and structures: a review, *Smart Mater. Struct.* 27 (2018) 023001.
- [32] Z. Wang, C. Luan, G. Liao, J. Liu, X. Yao, J. Fu, Progress in auxetic mechanical metamaterials: Structures, characteristics, manufacturing methods, and applications, *Adv. Eng. Mater.* 22 (2020) 2000312.
- [33] J.N. Grima, P.-S. Farrugia, R. Gatt, V. Zammit, Connected triangles exhibiting negative Poisson's ratios and negative thermal expansion, *J. Phys. Soc. Japan* 76 (2007) 025001.
- [34] L. Cabras, M. Brun, D. Misseroni, Micro-structured medium with large isotropic negative thermal expansion, *Proc. R. Soc. Lond. A* 475 (2019) 20190468.
- [35] J.S. Raminhos, J.P. Borges, A. Velinho, Development of polymeric anepctic meshes: auxetic metamaterials with negative thermal expansion, *Smart Mater. Struct.* 28 (2019) 045010.
- [36] Z. Lin, L.S. Novelino, H. Wei, N.A. Alderete, G.H. Paulino, H.D. Espinosa, S. Krishnaswamy, Folding at the microscale: Enabling multifunctional 3D origami-architected metamaterials, *Small* 16 (35) (2020) 2002229.
- [37] P.P. Pratapa, K. Liu, G.H. Paulino, Geometric mechanics of origami patterns exhibiting Poisson's ratio switch by breaking mountain and valley assignment, *Phys. Rev. Lett.* 122 (15) (2019) 155501.
- [38] P.P. Pratapa, K. Liu, S.P. Vasudevan, G.H. Paulino, Reprogrammable kinematic branches in tessellated origami structures, *J. Mech. Robot.* 13 (3) (2021) 031102.
- [39] J.N. Grima, R. Gatt, Perforated sheets exhibiting negative Poisson's ratios, *Adv. Eng. Mater.* 12 (6) (2010) 460–464.
- [40] X.C. Zhang, C.C. An, Z.F. Shen, H.X. Wu, W.G. Yang, J.P. Bai, Dynamic crushing responses of bio-inspired re-entrant auxetic honeycombs under in-plane impact loading, *Mater. Today Commun.* 23 (2020) 100918.
- [41] L. Francesconi, A. Baldi, X. Liang, F. Aymerich, M. Taylor, Variable Poisson's ratio materials for globally stable static and dynamic compression resistance, *Extreme Mech. Lett.* 26 (2019) 1–7.
- [42] L. Francesconi, A. Baldi, G. Dominguez, M. Taylor, An investigation of the enhanced fatigue performance of low-porosity auxetic metamaterials, *Exp. Mech.* 97 (2020) 93–107.
- [43] K.E. Evans, K.L. Alderson, Auxetic materials: the positive side of being negative, *Eng. Sci. Educ. J.* 9 (4) (2000) 148–154.
- [44] L. Mizzi, E. Salvati, A. Spaggiari, J.C. Tan, A.M. Korsunsky, Highly stretchable two-dimensional auxetic metamaterial sheets fabricated via direct-laser cutting, *Int. J. Mech. Sci.* 167 (2020) 105242.
- [45] A. Alderson, K.L. Alderson, Auxetic materials, *Proc. Inst. Mech. Eng. G* 221 (2007) 565–575.
- [46] A. Airoidi, P. Bettini, P. Panichelli, G. Sala, Chiral topologies for composite morphing structures –part II: novel configurations and technological processes, *Phys. Status Solidi b* 252 (2015) 1446–1454.
- [47] O. Duncan, T. Shepherd, C. Moroney, L. Foster, P.D. Venkatraman, K. Winwood, T. Allen, A. Alderson, Review of auxetic materials for sports applications: Expanding options in comfort and protection, *Appl. Sci.* 8 (2018) 941.
- [48] Q. Li, Y. Kuang, M. Zhu, Auxetic piezoelectric energy harvesters for increased electric power output, *AIP Adv.* 7 (2017) 015104.
- [49] S.K. Bhullar, J. Ko, F. Ahmed, M.B.G. Jun, Design and fabrication of stent with negative Poisson's ratio, *Int. J. Mech. Aerosp. Ind. Mechatron. Eng.* 8 (2014) 462–468.
- [50] W. Wu, X. Song, J. Liang, R. Xia, G. Qian, D. Fang, Mechanical properties of anti-tetrachiral auxetic stents, *Compos. Struct.* 185 (2018) 381–392.
- [51] R. Gatt, L. Mizzi, J.I. Azzopardi, K.M. Azzopardi, D. Attard, A. Casha, J. Briffa, J.N. Grima, Hierarchical auxetic mechanical metamaterials, *Sci. Rep.* 5 (2015) 8395.
- [52] H.M.A. Kolken, K. Lietaert, T. van der Sloten, B. Pouran, A. Meynen, G. Van Loock, H. Weinans, L. Scheys, A.A. Zadpoor, Mechanical performance of auxetic meta-biomaterials, *J. Mech. Behav. Biomed. Mater.* 104 (2020) 103658.
- [53] K.R. Olympio, F. Gandhi, Zero Poisson's ratio cellular honeycombs for flex skins undergoing one-dimensional morphing, *J. Intell. Mater. Syst. Struct.* 21 (2010) 1737–1753.
- [54] X. Gong, J. Huang, F. Scarpa, Y. Liu, J. Leng, Zero Poisson's ratio cellular structure for two-dimensional morphing applications, *Compos. Struct.* 134 (2015) 384–392.
- [55] G. Carta, L. Cabras, M. Brun, Continuous and discrete microstructured materials with null Poisson's ratio, *J. Eur. Ceram. Soc.* 36 (9) (2016) 2183–2192.
- [56] P. Fratzl, R. Weinkamer, Progress in materials, *Science* 52 (8) (2007) 1263–1334.
- [57] U. Wegst, H. Bai, E. Saiz, A.P. Tomsia, R.O. Ritchie, Bioinspired structural materials, *Nature Mater.* 14 (2015) 23–36.
- [58] F. Bosia, T. Abdalrahman, N.M. Pugno, Investigating the role of hierarchy on the strength of composite materials: evidence of a crucial synergy between hierarchy and material mixing, *Nanoscale* 4 (12) (2012) 1200–1207.
- [59] M. Grossman, D. Pivovarov, F. Bouville, C. Dransfeld, K. Masania, A.T. Studart, Hierarchical toughening of nacre-like composites, *Adv. Funct. Mater.* 29 (9) (2019) 1806800.
- [60] H. Gao, X. Wang, H. Yao, S. Gorb, E. Arzt, Mechanics of hierarchical adhesion structures of geckos, *Mech. Mater.* 37 (2–3) (2005) 275–285.
- [61] L. Brely, F. Bosia, N.M. Pugno, Emergence of the interplay between hierarchy and contact splitting in biological adhesion highlighted through a hierarchical shear lag model, *Soft Matter* 14 (26) (2018) 5509–5518.
- [62] G. Costagliola, F. Bosia, N.M. Pugno, Static and dynamic friction of hierarchical surfaces, *Phys. Rev. E* 94 (6–1) (2016) 063003.
- [63] M. Miniaci, A. Krushynska, A.S. Gliozzi, N. Kherraz, F. Bosia, N.M. Pugno, Design and fabrication of bioinspired hierarchical dissipative elastic metamaterials, *Phys. Rev. Appl.* 10 (2) (2018) 024012.
- [64] V.F. Dal Poggetto, F. Bosia, M. Miniaci, N.M. Pugno, Band gap enhancement in periodic frames using hierarchical structures, *Int. J. Solids Struct.* 216 (2021) 68–82.
- [65] B.W. Rosen, On some symmetry conditions for three dimensional fibrous composites, *J. Compos. Mater.* 5 (1971) 279–282.
- [66] R.M. Christensen, Sufficient symmetry conditions for isotropy of the elastic moduli tensor, *J. Appl. Mech.* 54 (1987) 772–777.